JVST B
Journal of Vacuum Science & Technology B

ARTICLE

avs.scitation.org/journal/jvb

Temperature dependent dielectric function and direct bandgap of Ge

Cite as: J. Vac. Sci. Technol. B 38, 012202 (2020); doi: 10.1116/1.5129685
Submitted: 30 September 2019 · Accepted: 20 November 2019 ·
Published Online: 18 December 2019

Carola Emminger,[1,a)] Farzin Abadizaman,[1] Nuwanjula S. Samarasingha,[1] Thomas E. Tiwald,[2] and Stefan Zollner[1]

AFFILIATIONS

[1]Department of Physics, New Mexico State University, P.O. Box 30001, Las Cruces, New Mexico 88003
[2]J. A. Woollam Co., Inc., 645 Main Street, Suite 102, Lincoln, Nebraska 68508

Note: This paper is part of the Conference Collection: 8th International Conference on Spectroscopic Ellipsometry 2019, ICSE.
[a)]**Electronic mail:** emminger@nmsu.edu

ABSTRACT

The dielectric function of bulk Ge is determined between 0.5 and 6.3 eV in a temperature range of 10–738 K using spectroscopic ellipsometry. The authors provide the data in a tabulated format that can be interpolated as a function of photon energy and temperature using commercial software. Another focus of this paper lies on the analysis of critical points, in particular, on the investigation of the temperature dependence of the direct bandgap E_0 and the critical point $E_0 + \Delta_0$, where Δ_0 is the spin–orbit splitting. To explore the temperature dependence of critical points, the parameters that characterize their line shapes are calculated using three different techniques. First, the common method of numerically calculating and analyzing the second derivatives of the dielectric function works well for critical points at higher energies. Second, an analysis in reciprocal space by performing a discrete Fourier transform and analyzing the resulting Fourier coefficients yields values for the energies of E_0 and $E_0 + \Delta_0$. Third, the energy determined from a parametric semiconductor model is shown as a function of temperature. The authors observe a temperature dependent redshift of the E_0 and $E_0 + \Delta_0$ critical point energies as well as an increase in the broadening of E_0 with temperature.

I. INTRODUCTION

Germanium, one of the most thoroughly studied semiconductors, is an indirect bandgap semiconductor having its indirect band edge at 0.66 eV[1] and its direct band edge at 0.8 eV[2,3] at room temperature. For the advancement of technologies and applications based on Ge, detailed knowledge of the optical constants and their temperature dependence is essential. Spectroscopic ellipsometry (SE) is a common method to measure optical constants, especially the dielectric function (DF) of materials.

Features such as peaks or shoulders in the DF are called critical points (CPs) and are related to interband transitions which take place at points or regions in the Brillouin zone (BZ) where the bands are parallel (Van Hove singularities).[4] The temperature dependence of CPs in Ge at energies above the bandgap (denoted E_1, $E_1 + \Delta_1$, E_0', $E_0' + \Delta_0'$, and E_2) was studied by Viña *et al.*[5] and Fernando *et al.*[6] Aspnes and Studna[7] used SE to determine the DF of Ge, Si, and several III–V semiconductors at room temperature. The DF of Ge at various temperatures was measured between 100 and 850 K from 1.25 to 5.6 eV[5] and between 80 and 780 K from 0.8 to 6.5 eV[6] using SE.

The dependence on temperature of the direct bandgap energy was examined by McLean[8] and Varshni[9] for Ge and other semiconductors. The E_0 energies of Ge were also measured at 1.5, 77, and 293 K by magnetoabsorption;[10] at 24, 89, and 305 K by electroabsorption;[11] at 10 K by electroreflectance;[12] at 20 K by optical transmission;[13] and at 300 K by piezoreflectance[14] and electroreflectance.[15] The spin–orbit splitting Δ_0 was obtained at 4, 10, 24, 30, and 300 K using various techniques.[12,16–19] Hobden[2] and McLean and Paige[20,21] studied the temperature dependence of the broadening of the direct and indirect bandgaps from liquid helium temperature to 400 K.

The present work provides the DF of bulk Ge between 10 and 738 K with approximately 25 K steps measured by SE from 0.5 to 6.3 eV, including the direct band edges E_0 and $E_0 + \Delta_0$. We are especially interested in the effect of temperature on these two CPs. To quantitatively analyze the temperature behavior of interband transitions, the parameters that describe the line shape of CPs are

evaluated. The second derivatives of the real and imaginary parts of the dielectric function around the CP can be calculated using a Savitzky–Golay[22] algorithm and fitted to determine the CP parameters.[5,6,23] Another approach established by Aspnes and Yoo[24–27] is to perform a discrete Fourier transform of the data points in the region of the CP and to fit the resulting Fourier coefficients. We present the results for the energies of E_0 and $E_0 + \Delta_0$ as a function of temperature and discuss the temperature effect on the broadening of E_0.

II. EXPERIMENTAL METHODS

A. Sample preparation

We used a commercially obtained undoped bulk Ge wafer of (100) surface orientation with a resistivity greater than 40 Ω cm. To reduce and stabilize the native oxide layer on the top of the Ge bulk substrate, a cleaning procedure was applied to the sample similar to the approach described elsewhere.[6,28] First, the sample was cleaned ultrasonically in ultrapure water for 20 min and then in isopropanol for another 20 min. Next, an ozone clean as described in Ref. 28 with 2 min oxygen flow, 20 min heating at 150 °C, and an incubation period of 30 min was performed. Finally, the first step (water and isopropanol) was repeated. Immediately after cleaning, the sample was mounted into a UHV cryostat to avoid oxidation. Once under vacuum, the sample was heated up and kept at a temperature of 700 K for several hours to allow for degassing and further stabilization of the oxide. The resulting thickness of the oxide layer determined from SE measurements (described below) was found to be 10 ± 1 Å over the whole temperature range between 10 and 738 K. The oxide thickness at each temperature is plotted in Fig. S2.[47]

B. Ellipsometry measurements

The pseudodielectric function (pseudo-DF) of the Ge substrate was determined between 0.5 and 6.3 eV from the ellipsometric angles Ψ and Δ measured by a J. A. Woollam VASE ellipsometer[29] at 31 different temperatures between 10 and 738 K. The results are plotted in Fig. S1 (Ref. 47) showing the change of the pseudo-DF as the temperature increases. To produce a sufficiently high vacuum and to measure at very low and high temperatures, the sample was mounted into a UHV cryostat as described in Ref. 6. To record the temperature of the sample, a type-E thermocouple was attached directly to the sample surface. Due to the construction of the cryostat, the angle of incidence is fixed to 70°.

Using liquid helium, a temperature of about 10 K was achieved. Liquid nitrogen was utilized together with a heater connected to the cryostat to measure at temperatures between 80 K and room temperature. Measurements were taken in the range between 0.7 and 6.3 eV with 10 meV steps using a xenon light source, where each measurement in that range took about three hours for the chosen step size. Due to the limitations of the glass fiber, separate measurements were performed in the infrared between 0.5 and 3 eV using a quartz tungsten halogen lamp and a suitable glass fiber for this energy range. A measurement in this range takes about 1.5 h for a step size of 10 meV. The data were found to be in good agreement and could be merged in the overlap region of 0.7–3 eV.

At the liquid helium and liquid nitrogen temperatures, measurements with slit widths of 500 μm, 1 mm, and 2 mm and step sizes of 0.5 and 1 meV were performed between 0.5 and 3 eV to resolve the narrow structure of the direct bandgap. Additional measurements were taken using a slit width of 500 μm and a step size of 2 meV at temperatures between 110 and 718 K in the range of E_0 and $E_0 + \Delta_0$ to determine the temperature dependence of these two CPs. Depending on the bandgap energy, the spectral resolution of the instrument with respect to the choice of the slit width is between 1 and 2 meV. At temperatures above 500 K, we placed an iris right after the exit window of the cryostat to suppress effects of blackbody radiation in the low energy region [see Fig. S4 (Ref. 47)].

III. RESULTS AND DATA ANALYSIS

To obtain the DF from the pseudodielectric one, the data were corrected for the native oxide layer as explained in Ref. 6 by fitting Δ in the region below the bandgap to determine the oxide layer thickness using the optical constants for GeO_2 taken from the literature.[28] The results for the real and imaginary parts of the DF at temperatures between 10 and 738 K are shown in Fig. 1 with the arrows indicating the changes due to increasing temperature.

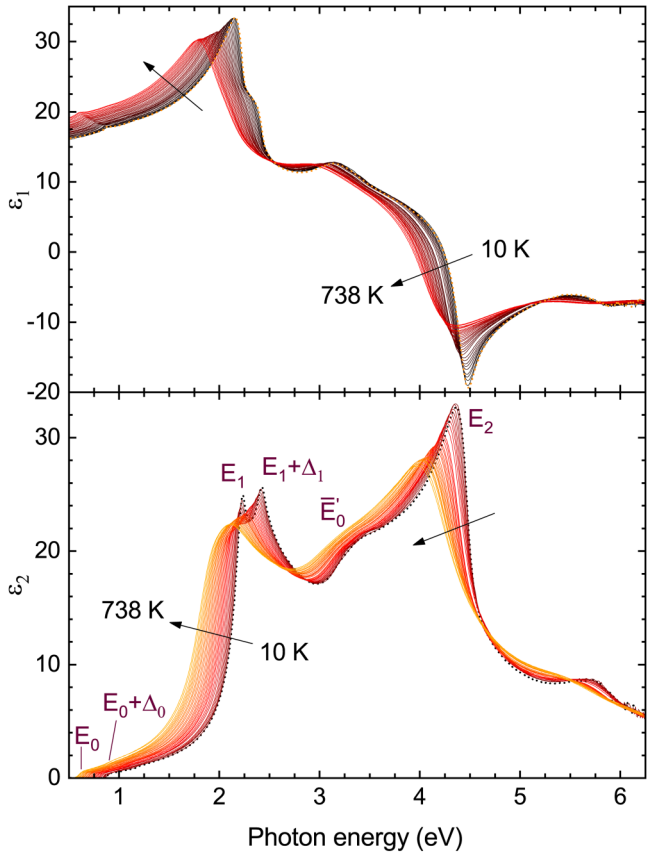

FIG. 1. Real (ϵ_1) and imaginary (ϵ_2) parts of the dielectric function of bulk Ge from 10 to 738 K. The arrows indicate changes from the measurement at 10 (dotted) to 738 K.

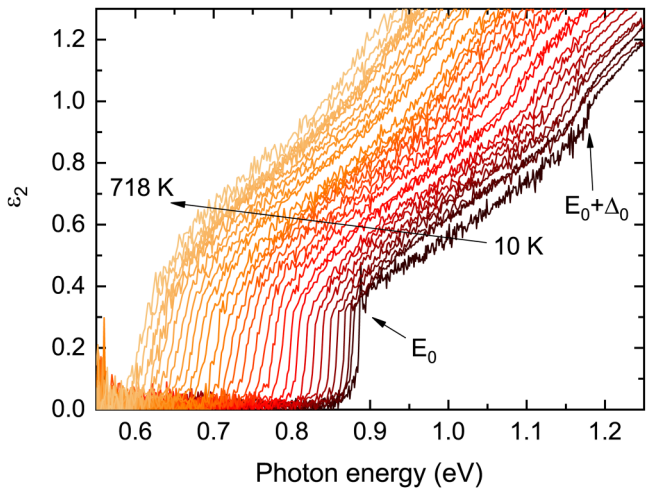

FIG. 2. Real part of the dielectric function of bulk Ge from 10 to 718 K using a step size of 1 meV (10 K) and 2 meV (80–718 K) and a slit width of 500 μm. The arrow indicates changes from the measurement due to temperature.

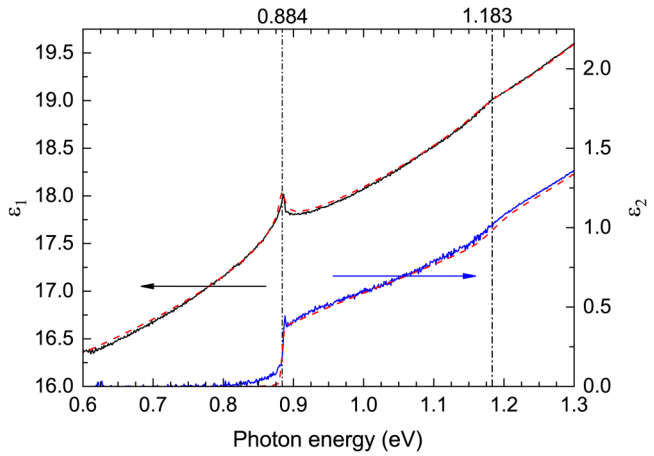

FIG. 3. Real and imaginary parts of the dielectric function of Ge at 10 K. The solid lines show an independent fit at each photon energy, and the dashed lines show the fit by a parametric semiconductor model after performing an oxide correction.

It can be seen from Fig. 1 that the structures in the DF redshift as the temperature rises. Furthermore, a change in broadening and amplitude of the CPs is observable. The CPs in the investigated spectra of the DF are the direct band edges E_0 and $E_0+\Delta_0$ below 1 eV (corresponding to interband transitions at the Γ point of the BZ), E_1 and $E_1+\Delta_1$ between 1.5 and 2.5 eV [transitions along the (111) direction], E_0' and $E_0'+\Delta_0'$ between 3 and 3.7 eV [transitions along the (100) direction] and E_2 between 3.8 and 5 eV (transitions close to the X-point).[30,31] Since E_0' and $E_0'+\Delta_0'$ can hardly be resolved, we treat them as one CP denoted here as E_0'.

Figure 2 shows the imaginary part of the DF in the range from 0.55 to 1.25 eV in greater detail to focus on the E_0 and $E_0+\Delta_0$ absorption edges. One observes that both CPs redshift and broaden with increasing temperature. At the lowest temperatures, an excitonic enhancement is present at the E_0 gap which is also demonstrated in Fig. 3 showing the real and imaginary parts of the DF at 10 K together with a fit using the parametric semiconductor model[32] after performing an oxide correction.

Two different detectors are used for the UV–VIS range and the near-IR range, which are switched at 1.18 eV. This detector change caused a 0.06° step in Ψ, probably due to a very small angle offset. The CP $E_0+\Delta_0$ has its threshold energy at about 1.18 eV at 10 K; therefore, we had to manually remove the step caused by the instrument before fitting the data at 10 K.

A. Temperature model

The DFs of Ge at each temperature were combined into a single model describing the DF as a function of temperature. The model was built in the following manner:[33] First, B-splines were used to smooth the constituent DF—one for each of the 31 different temperatures—and these spectra were combined in a single temperature library file. For a given temperature, the DF is determined by the interpolation between the nearest reference spectra. The underlying interpolation algorithm for the library is based on the critical point shifting algorithm of Snyder *et al.*[34] In this algorithm, the DF at an arbitrary temperature (or composition) is evaluated from a weighted sum of the nearest reference dielectric function spectra, after the reference spectra are wavelength shifted to line up the critical point features. Polynomials describing the critical point positions vs composition are automatically determined via a nonlinear regression analysis as part of the temperature library file building process.

B. Critical point analysis

The line shape of the DF around a CP can be described by[5]

$$\epsilon(\omega) = B - \frac{Ae^{i\phi}}{(\hbar\omega - E_g + i\Gamma)^{\mu}}, \tag{1}$$

where the CP parameters are the amplitude A, the broadening Γ, the threshold energy E_g, and the phase angle ϕ which describes excitonic effects by mixing the real and imaginary parts and characterizes the type of CP.[5] The parameter B is a nonresonant background. The order of the singularity is defined by the exponent μ, where $\mu=1$ for an excitonic (0D) line shape, $\mu=0.5$ for a one-dimensional (1D), $\mu=0$ for a 2D with $\epsilon(\omega)\propto\ln(\hbar\omega-E+i\Gamma)$, and $\mu=-0.5$ for a 3D line shape.[5,31] The latter describes the DF at the direct bandgap and was, therefore, used for the analysis described in Secs. III B 1 and III B 2.

1. Analysis in direct space

A common method to find CP parameters is to analyze the second derivatives (SDs) of the real (ϵ_1) and imaginary (ϵ_2) parts of the DF.[5,6] The derivatives $d^2\epsilon_1/dE^2$ and $d^2\epsilon_2/dE^2$ are calculated numerically and smoothed using a Savitzky–Golay[22] algorithm. This method works well for CPs of Ge at higher energies, such as E_1 and

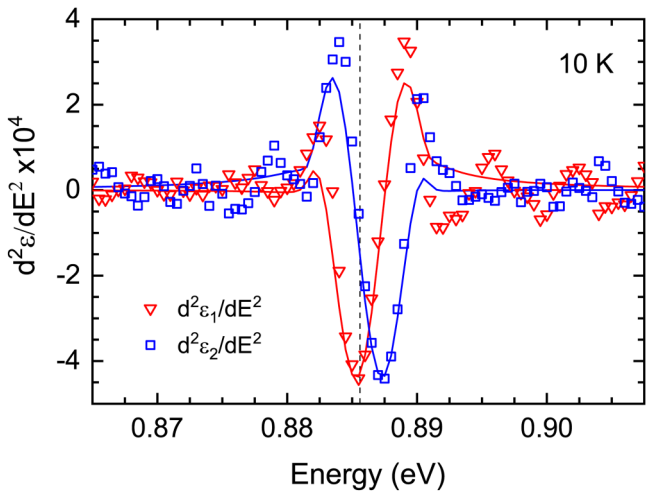

FIG. 4. Numerically calculated second derivatives of the real part (triangles) and the imaginary part (squares) of the dielectric function of Ge at 10 K. The solid lines represent the best fit to the data, and the vertical dashed line indicates the E_0 threshold energy.

$E_1 + \Delta_1$, as demonstrated in Fig. S8 (Ref. 47) showing $d^2\epsilon_1/dE^2$ and $d^2\epsilon_2/dE^2$ at 10 K together with the best fit to the data points.

For the direct bandgap, the SDs of ϵ_1 and ϵ_2 using a 3D line shape and the best fits to the data are shown in Fig. 4 at 10 K. Apparently, the deviation of the fits from the data is larger than in Fig. S8,[47] which might be due to assuming a 3D line shape in spite of the fact that it is not a perfect description for the direct edge in Ge since it ignores the excitonic enhancement that is present at low temperatures. Despite this discrepancy, reasonable values for the energy and broadening of E_0 are found and discussed in Sec. III D.

More challenging is the case of the $E_0 + \Delta_0$ transition due to the weak and broad structure of this CP. We could not find a distinct peak corresponding to $E_0 + \Delta_0$ in the spectra of $d^2\epsilon_1/dE^2$ and $d^2\epsilon_2/dE^2$ for the data sets at most temperatures. Another way to extract the energies of CPs, which was not implemented here, is the method of symmetrized lineshapes explained in Ref. 35.

2. Analysis in reciprocal space

The second method we used to analyze the line shapes of CPs is an analysis in RS by performing a discrete Fourier transform of the data points and fitting the resulting Fourier coefficients.[24–27] This method is applied to our data to find the energies of E_0 and $E_0 + \Delta_0$.

In the first step, a segment of the spectrum of either the real or the imaginary part of the DF containing one CP of interest providing a sufficiently large number of data points (200 or more worked well for our data) is chosen. Next, a discrete Fourier transform of the M data points d_j (either $\epsilon_{1,j}$ or $\epsilon_{2,j}$) in the segment yields the Fourier coefficients expressed as a phase ξ_n and an amplitude C_n,[27]

$$d_j = Re\left[\sum_{n=0}^{N_{max}} C_n e^{-i\xi_n} e^{in\theta_j}\right], \tag{2}$$

where

$$1 \le j \le M, \tag{3}$$

$$\theta_j = \frac{2\pi}{M}(j - j_i), \tag{4}$$

and the inversion origin $j_i = (j_1 + j_M)/2$, with j_1 and j_M defining the first and the last data point of the segment, respectively, and $N_{\max} = \mathrm{Int}(M/2)$. To avoid artifacts due to discontinuities at the endpoints of the segment, the procedure explained in Ref. 27 is applied to calculate the phases ξ_n, which are used to find the energy of the CP via the relation[27]

$$\xi_n = -\mu\frac{\pi}{2} - \phi + n\frac{E_g - E_i}{\Delta E}, \tag{5}$$

with parameters μ, ϕ, and E_g defined in Eq. (1),

$$\Delta E = \frac{E_M - E_1}{M - 1}\frac{M}{2\pi}, \tag{6}$$

$$E_i = [E_1(M - j_i) + E_M(j_i - 1)]/(M - 1), \tag{7}$$

where E_1 (not to be confused with the CP E_1) and E_M are the lowest and the highest energy in the segment, respectively. By fitting ξ_n calculated from the DF to Eq. (5), one can find the phase angle ϕ and the CP energy E_g. The latter is found by shifting E_i until ξ_n in Eq. (5) is independent of n, which yields an accurate value for the position of the CP.

Figure 5 shows the phases ξ_n obtained from the RS analysis applied to the real part of the DF at 10 K with a step size of 1 meV

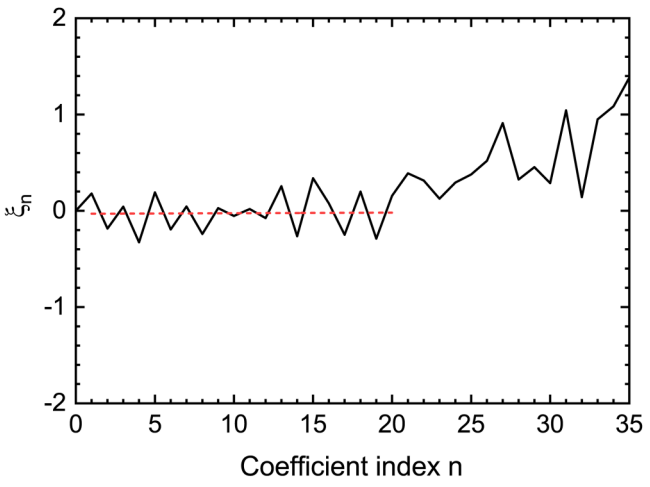

FIG. 5. Phase ξ_n of the Fourier coefficients obtained from a reciprocal space analysis of the real part of the dielectric function at 10 K with a step size of 1 meV and a slit width of 0.5 mm. The dashed line shows the fit to the mid-index Fourier coefficients using Eq. (5).

and a slit width of 0.5 mm. The chosen segment starts at 0.8 eV and ends at 1 eV, which provides 200 data points for the discrete Fourier transform. The onset of the white noise range is at $n = 20$, and the fitting range for ξ_n is chosen accordingly. The position of the CP is determined by minimizing the slope of ξ_n, which gives the CP energy $E_0 = (0.886 \pm 0.001)$ eV.

C. Parametric semiconductor model

Eight oscillators were used to fit the Ge data with the parametric semiconductor (PS) model[32] at each temperature, one oscillator for each CP (E_0, $E_0 + \Delta_0$, E_1, $E_1 + \Delta_1$, $\tilde{E}_0'$, and E_2), one for the small peak between 5 and 6 eV, and one outside of the measured range to ensure the Kramers–Kronig consistency. The threshold energy, the broadening, and the amplitude were fitted for each CP. From this parametric oscillator fit, the E_0 and $E_0 + \Delta_0$ energies were found at each measured temperature and compared to the results from the analysis methods explained above. At some temperatures, the shape parameters of the PS model were adjusted to achieve a good fit.

D. Temperature dependence of E_0 and $E_0 + \Delta_0$

The CP energies shift with increasing temperature due to thermal expansion of the crystal lattice and renormalization of the band energies due to electron–phonon interactions.[36] The electron–phonon contribution is calculated theoretically in Ref. 37 for the direct bandgaps in Si and Ge using a Debye–Waller[14,38] and a self-energy term.[39]

By using a Bose–Einstein statistical factor, the temperature dependence due to electron–phonon interactions can be described as[5,36]

$$E(T) = E_a - E_b\left[1 + 2/\left(e^{\theta_B/T} - 1\right)\right], \tag{8}$$

where E_a is the unrenormalized transition energy, E_b is the electron–phonon coupling strength, and θ_B multiplied by the Boltzmann constant k_B is the effective phonon energy. A similar expression is used for the temperature dependence of the broadening of CPs,[5]

$$\Gamma(T) = \Gamma_1 + \Gamma_0\left[1 + 2/\left(e^{\theta_B/T} - 1\right)\right]. \tag{9}$$

In Fig. 6, the energies of the CPs E_0 and $E_0 + \Delta_0$ are plotted at each temperature between 10 and 738 K using the three different analysis methods described above. Equation (8) is fitted to the temperature dependent energies and represented by the various lines in the graph. We do not subtract the term describing the temperature effect due to thermal expansion. Since excitonic effects are ignored in our analysis, the resulting energies are suspected to be slightly smaller than the single particle energy. This difference is on the order of meV, the binding energy of excitons at the Γ point.

The PS model was used to find the $E_0 + \Delta_0$ energies up to 680 K, and the RS analysis yields the energies up to 325 K. Above 680 K, the structure becomes too broad to be fitted with the PS model. In the case of the RS analysis, the onset of the white noise

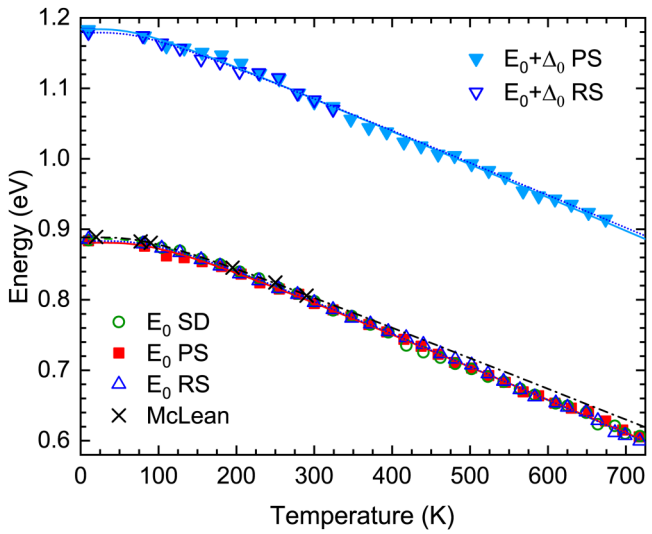

FIG. 6. Temperature dependence of the E_0 and $E_0 + \Delta_0$ energies determined by a parametric semiconductor (PS) model, a second derivative (SD), and an RS analysis compared to the results from Ref. 8 (McLean). The lines show the fit to the data using Eq. (8) with parameters given in Table I for the PS (solid), SD (dashed), RS (dotted), and the McLean (dashed–dotted) results.

range shifts toward lower Fourier indices with rising temperature, which means that there are not enough data points available in the range of the mid-index Fourier coefficients to allow for a good fit in the case of the DF data sets above 325 K.

Using the results of the energies from the PS model, the spin–orbit splitting Δ_0 is calculated at temperatures between 10 and 680 K and shown in Fig. 7 together with Δ_0 determined from the RS analysis between 10 and 325 K. The error bars were obtained from a uniqueness fit[40] to confirm that the PS model is sensitive to the E_0 and $E_0 + \Delta_0$ energies. The average and standard deviation of the spin–orbit splitting determined from the PS model are found to be $\Delta_0 = (290 \pm 7)$ meV, in good agreement with values from band structure calculations[41] and experimental work.[12,16–19] The ratio of the splitting Δ_1 and the direct edge splitting is about 0.69, which is consistent with the two-third rule stated in Ref. 30.

Table I lists the fitting parameters of Eq. (8) for all CPs in the measured spectrum of the DF of Ge obtained from the three analysis methods explained above and compared to the results from Refs. 5 and 6. The effective phonon energies E_{ph} listed in the table suggest that acoustic phonons (the phonon energy is 28 meV for longitudinal acoustic phonons and 8 meV for transverse acoustic phonons)[42,43] are involved in the electron–phonon interaction process with E_0 and $E_0 + \Delta_0$.

The analysis of the broadening of the direct bandgap is more challenging than finding the energies. Figure 8 shows an overall increase with the temperature of the broadening of E_0, which was evaluated using the SD method. The dots in Fig. 8 show the spectral resolution of the monochromator caused by the grating used in this energy range ($\Delta\lambda = 4.6$ nm/mm), calculated using the E_0 energies obtained from the RS analysis at the measured temperatures

TABLE I. Parameters E_a, E_b, θ_B, and the effective phonon energy E_{ph} obtained from fitting Eq. (8) to the temperature dependent energies of E_0, $E_0 + \Delta_0$, E_1, $E_1 + \Delta_1$, E_0', and E_2 critical points. The E_0 and $E_0 + \Delta_0$ energies are fitted using the parametric semiconductor model (PS), the analysis in RS, and the second derivative (SD) method. The parameters marked (f) of Ref. 6 was fixed during the fit.

	E_a (eV)	E_b (eV)	θ_B (K)	$E_{ph} = k_B \cdot \theta_B$ (meV)
E_0 (PS)[a]	0.945 ± 0.003	0.067 ± 0.004	284 ± 13	24 ± 1
E_0 (RS)[a]	0.953 ± 0.003	0.070 ± 0.004	290 ± 16	25 ± 1
E_0 (SD)[a]	0.947 ± 0.004	0.061 ± 0.005	256 ± 20	22 ± 2
E_0 (Ref. 8)	0.943 ± 0.007	0.054 ± 0.008	245 ± 25	21 ± 2
$E_0 + \Delta_0$ (PS)[a]	1.233 ± 0.006	0.049 ± 0.009	207 ± 35	18 ± 3
$E_0 + \Delta_0$ (RS)[a]	1.23 ± 0.02	0.05 ± 0.02	225 ± 58	19 ± 5
E_1[a]	2.292 ± 0.002	0.059 ± 0.003	198 ± 10	17 ± 1
E_1 (Ref. 6)	2.295 ± 0.002	0.063 ± 0.004	218 ± 14	19 ± 1
E_1 (Ref. 5)	2.33 ± 0.03	0.12 ± 0.04	360 ± 120	31 ± 10
$E_1 + \Delta_1$[a]	2.494 ± 0.002	0.064 ± 0.003	213 ± 9	19 ± 1
$E_1 + \Delta_1$ (Ref. 6)	2.494 ± 0.002	0.064 ± 0.001	218 (f)	19 (f)
E_0'[a]	3.34 ± 0.02	0.15 ± 0.02	581 ± 42	50 ± 4
E_0' (Ref. 6)	3.18 ± 0.02	0.05 ± 0.02	313 ± 107	27 ± 9
E_0' (Ref. 5)	3.23 ± 0.02	0.08 ± 0.03	484 ± 136	42 ± 12
E_2[a]	4.508 ± 0.006	0.04 ± 0.01	169 ± 41	15 ± 4
E_2 (Ref. 6)	4.505 ± 0.006	0.05 ± 0.01	217 ± 41	19 ± 4
E_2 (Ref. 5)	4.63 ± 0.05	0.17 ± 0.06	499 ± 127	43 ± 11

[a]Present work.

(Δ in Fig. 6) via $\Delta E = (hc/\lambda^2)\Delta\lambda$, where λ is the direct gap wavelength in nanometers. Below room temperature, the broadening appears to be purely instrumental. Equation (9) is fitted to the data between 279 and 686 K, ignoring the values below room temperature due to the limitation of the spectral resolution and the ones at the highest temperatures which might be inaccurate due to noise in the data. The fitting parameters corresponding to Eq. (9) are $\Gamma_1 = 0$ meV, $\Gamma_0 = 0.8$ meV and $\theta_B = 167$ K ($E_{ph} = 14$ meV).

From the large variation of the broadening parameters above 450 K, we conclude that the SD method is not sensitive to the broadening at higher temperatures, probably due to the increase of noise since the values also vary with the number of smoothing

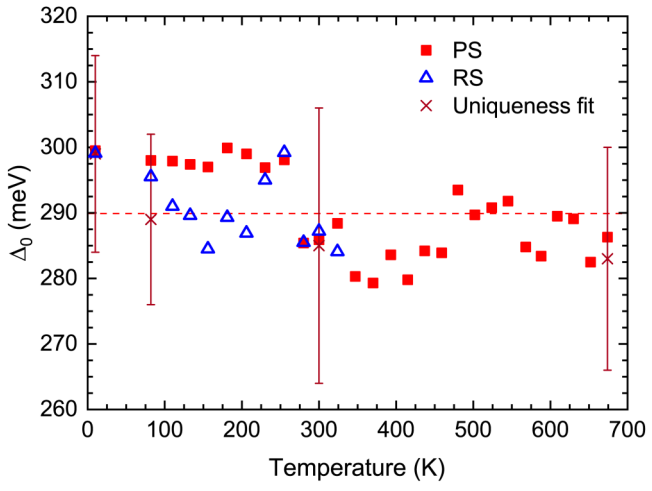

FIG. 7. Temperature dependence of the spin–orbit splitting Δ_0 determined by a parametric semiconductor (PS) model and an RS analysis. A uniqueness fit was performed to determine error bars at certain temperatures. The dashed line shows the average of the PS splitting.

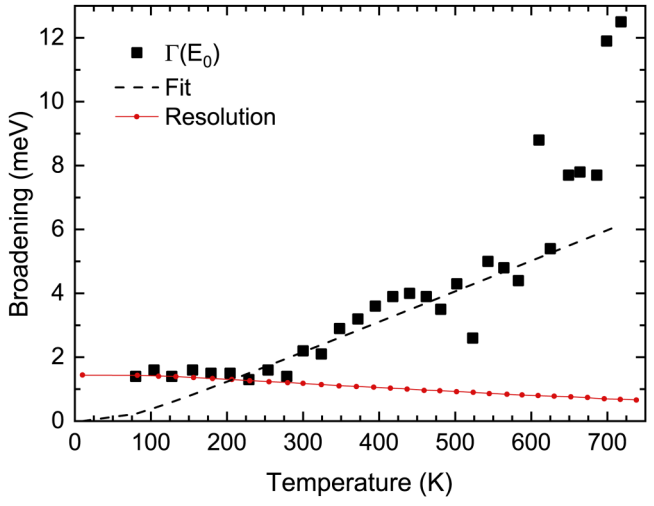

FIG. 8. Temperature dependence of the broadening of the E_0 edge determined from the second derivatives analysis. The dashed line represents the best fit to the data between 279 and 686 K using Eq. (9). The dots show the calculated resolution of the monochromator at the E_0 energies in Fig. 6.

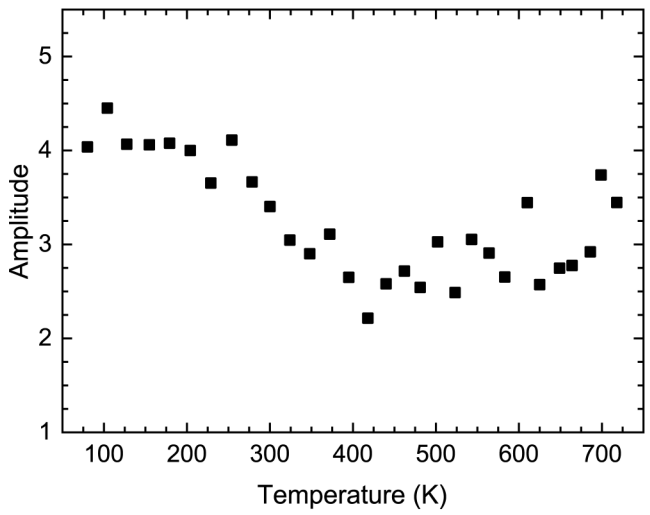

FIG. 9. Amplitude of the E_0 edge determined from the second derivatives analysis at each measured temperature.

coefficients. Similarly, the SD fit is not sensitive to the broadening at 10 K and yields a value which is significantly smaller than the spectral resolution. The broadening parameter at 256 and 300 K, however, are in reasonable agreement with the values presented in Ref. 21 at 250 and 290 K, respectively.

The broadening of the E_0 critical point of Ge is primarily determined by the lifetime of electrons at the Γ point, which is given by the intervalley scattering rate of electrons from Γ to the L-valley by absorption or emission of phonons. Ignoring the influence of spin–orbit splitting effects on intervalley scattering, the electrons in the center of the BZ have Γ_2' symmetry, while those in the L-valley have an approximate L_1 symmetry. As explained by Birman,[44] only L_2' (longitudinal acoustic) phonons can mediate transitions between Γ_2' and L_1, but due to the difference in the Γ_2' and L_1 energies, smaller contributions can also arise from transverse phonons.[45,46] At room temperature, a broadening of 2 meV corresponds to a Γ to L intervalley scattering time of about $\tau = \hbar/2\Gamma = 165$ fs.

The amplitudes of the E_0 CP shown in Fig. 9 were determined from the SD analysis and are found to vary between 2 and 4.5. Below room temperature, the amplitudes are larger than the values at higher temperatures, which can be explained by the fact that the amplitude values obtained from the SD analysis are scaled by the corresponding broadening. Since the broadening is limited by the spectral resolution at low temperatures, the amplitudes appear to be larger. For example, multiplying the amplitude at 80 K by a broadening of 1 meV instead of 1.4 meV results in a value of 2.8 instead. Considering these facts, we conclude that the amplitudes do not show a temperature dependence, similar to the results for other CPs [see Fig. S12 (Ref. 47) and Refs. 5 and 6].

IV. SUMMARY

The dielectric function of Ge was measured using spectroscopic ellipsometry between 0.5 and 6.3 eV at temperatures ranging from 10 to 738 K (in 25 K steps) to determine the temperature dependence of critical points, focusing on the direct band edges E_0 and $E_0 + \Delta_0$. We found a redshift with increasing temperature for the E_0 and $E_0 + \Delta_0$ energies which were determined from a parametric semiconductor model, an analysis of the second derivatives of the dielectric function, and an analysis in reciprocal space by performing a discrete Fourier transform. The spin-orbit splitting $\Delta_0 = (0.290 \pm 0.007)$ eV turns out to be independent of temperature and the ratio between the splittings Δ_1 and Δ_0 is about two thirds, as expected.[30] Moreover, an increase of the broadening of the direct bandgap with temperature was observed while the amplitudes are found to be independent of temperature. Further research is suggested to allow for a more detailed analysis of the E_0 CP parameters by taking into account excitonic effects and find corrected values of the energies. The limitation in the spectral resolution needs to be overcome to achieve an accurate description of the temperature dependent broadening below room temperature.

ACKNOWLEDGMENTS

The authors would like to thank D. E. Aspnes for his help with the application of the reciprocal space analysis. This work was supported by the J. A. Woollam Company, the National Science Foundation (NSF, No. DMR-1505172), and the Austrian Marshall Plan Foundation.

REFERENCES

[1]G. G. Macfarlane, T. P. McLean, J. E. Quarrington, and V. Roberts, Phys. Rev. **108**, 1377 (1957).
[2]M. Hobden, J. Phys. Chem. Solids **23**, 821 (1962).
[3]M. Rouzeyre, H. Mathieu, D. Auvergne, and J. Camassel, Solid State Commun. 7, 1219 (1969).
[4]L. Van Hove, Phys. Rev. **89**, 1189 (1953).
[5]L. Viña, S. Logothetidis, and M. Cardona, Phys. Rev. B **30**, 1979 (1984).
[6]N. S. Fernando *et al.*, Appl. Surf. Sci. **421**, 905 (2017).
[7]D. E. Aspnes and A. A. Studna, Phys. Rev. B **27**, 985 (1983).
[8]T. P. McLean, *Progress in Semiconductors*, edited by A. F. Gibson (Heywood, London, 1960), Vol. 5.
[9]Y. P. Varshni, Physica **34**, 149 (1967).
[10]S. Zwerdling, B. Lax, L. M. Roth, and K. J. Button, Phys. Rev. **114**, 80 (1959).
[11]A. Frova and C. M. Penchina, Phys. Status Solidi B **9**, 767 (1965).
[12]D. E. Aspnes, Phys. Rev. B **12**, 2297 (1975).
[13]T. P. McLean and E. G. S. Paige, J. Phys. Chem. Solids **18**, 139 (1961).
[14]J. Camassel and D. Auvergne, Phys. Rev. B **12**, 3258 (1975).
[15]D. E. Aspnes, Surf. Sci. **37**, 418 (1973).
[16]M. V. Hobalen, J. Phys. Chem. Solids **23**, 821 (1962).
[17]T. Nishino and Y. Hamakawa, J. Phys. Soc. Jpn. **26**, 403 (1969).
[18]R. L. Aggarwal, Phys. Rev. B **2**, 446 (1970).
[19]S. H. Groves, C. R. Pidgeon, and J. Feinleib, Phys. Rev. Lett. **17**, 446 (1966).
[20]T. P. McLean and E. G. S. Paige, J. Phys. Chem. Solids **23**, 822 (1962).
[21]T. P. McLean and E. G. S. Paige, *Proceedings of the International Conference on the Physics of Semiconductors, Exeter*, edited by A. C. Stickland (The Institute of Physics and The Physical Society, London, 1962), p. 450.
[22]A. Savitzky and M. J. E. Golay, Anal. Chem. **36**, 1627 (1964).
[23]S. Zollner, M. Garriga, J. Kircher, J. Humlíček, M. Cardona, and G. Neuhold, Phys. Rev. B **48**, 7915 (1993).
[24]S. D. Yoo, D. E. Aspnes, S. J. Rhee, and J. C. Woo, Appl. Phys. Lett. **68**, 3230 (1996).
[25]D. E. Aspnes and S. D. Yoo, Phys. Status Solidi B **215**, 715 (1999).

[26]S. D. Yoo, D. E. Aspnes, L. F. Lastras-Martínez, T. Ruf, M. Konuma, and M. Cardona, Phys. Status Solidi B **220**, 117 (2000).
[27]S. D. Yoo and D. E. Aspnes, J. Appl. Phys. **89**, 8183 (2001).
[28]T. N. Nunley, N. S. Fernando, N. Samarasingha, J. M. Moya, C. M. Nelson, A. A. Medina, and S. Zollner, J. Vac. Sci. Technol. B **34**, 061205 (2016).
[29]J. A. Woollam Co., Inc., Lincoln, NE. Model V-VASE.
[30]M. Cardona and G. Harbeke, J. Appl. Phys. **34**, 813 (1963).
[31]P. Y. Yu and M. Cardona, *Fundamentals of Semiconductors: Physics and Materials Properties* (Springer, Berlin, 1996).
[32]C. M. Herzinger and B. Johs, U.S. patent 5,796,983 (18 August 1998).
[33]B. Johs and J. S. Hale, Phys. Status Solidi A **205**, 715 (2008).
[34]P. G. Snyder, J. A. Woollam, S. A. Alterovitz, and B. Johs, J. Appl Phys. **68**, 5925 (1990).
[35]O. Caha, P. Kostelník, J. Šik, Y. D. Kim, and J. Humlíček, Appl. Phys. Lett. **103**, 202107 (2013).
[36]P. Lautenschlager, P. B. Allen, and M. Cardona, Phys. Rev. B **31**, 2163 (1985).
[37]P. B. Allen and M. Cardona, Phys. Rev. B **27**, 4760 (1983).
[38]E. Antončík, Czech. J. Phys. **5**, 449 (1955).
[39]H. Y. Fan, Phys. Rev. **82**, 900 (1951).
[40]J. N. Hilfiker, N. Singh, T. Tiwald, D. Convey, S. M. Smith, J. H. Baker, and H. G. Tompkins, Thin Solid Films **516**, 7979 (2008).
[41]E. O. Kane, J. Phys. Chem. Solids **1**, 82 (1956).
[42]W. Weber, Phys. Rev. B **15**, 4789 (1977).
[43]G. G. Macfarlane, T. P. McLean, J. E. Quarrington, and V. Roberts, J. Phys. Chem. Solids **8**, 388 (1959).
[44]J. L. Birman, Phys. Rev. **127**, 1093 (1962).
[45]M. Lax and J. J. Hopfield, Phys. Rev. **124**, 115 (1961).
[46]T. Nishino, M. Takeda, and Y. Hamakawa, J. Phys. Soc. Jpn. **37**, 1016 (1974).
[47]See supplementary material at http://dx.doi.org/10.1116/1.5129685 for additional discussion of the experimental methods todetermine the oxide thickness and the dielectric function (DF) from the pseudo-DF, as well as experimental issues arising from blackbody radiation in the bandgap region at high temperatures. Furthermore, difficulties in the analysis in reciprocal space in the case of three-dimensional line shapes are addressed. The E_0 and $E_0 + \Delta_0$ energies are plotted as a function of temperature using Varshni's equation. Finally, results of the CP analysis for E_1 and $E_1 + \Delta_1$ are presented and compared to Refs. 5 and 6.

Supplementary Material: Temperature dependent dielectric function and direct band gap of Ge

(Dated: 20 November 2019)

Carola Emminger,[1] Farzin Abadizaman,[1] Nuwanjula S. Samarasingha,[1] Thomas E. Tiwald,[2] and Stefan Zollner[1]
[1)] *Department of Physics, New Mexico State University, P.O. Box 30001, Las Cruces, NM 88003, USA*
[2)] *J. A. Woollam Co., Inc., 645 Main Street, Suite 102, Lincoln, NE 68508, USA*

S1. EXPERIMENTAL METHODS

The real $\langle\epsilon_1\rangle$ and imaginary $\langle\epsilon_2\rangle$ parts of the pseudo-DF at temperatures between 10 K and 738 K are shown in Fig. S1 together with the DF. As explained in Sec. II, the pseudo-DF is corrected for the native oxide thickness to determine the DF, depicted in Fig. 1 of the main text.

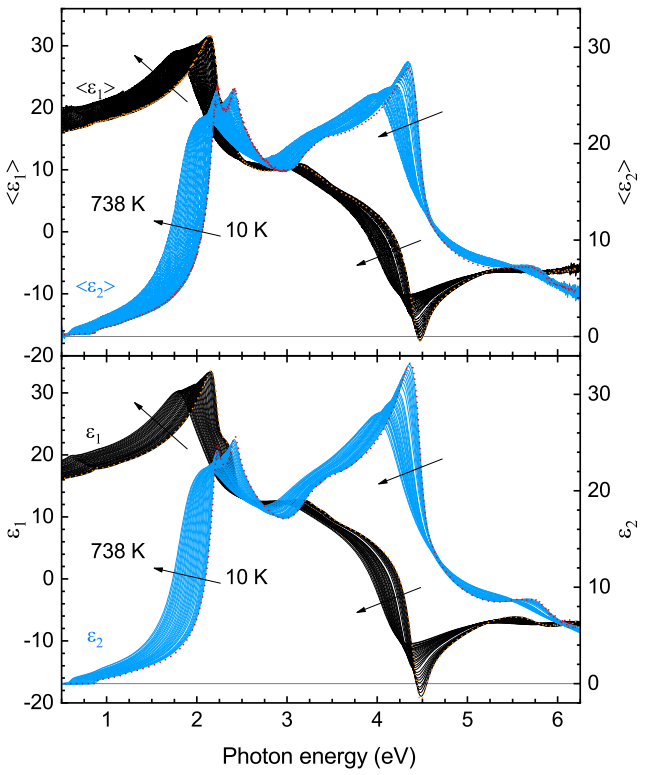

FIG. S1. Temperature dependence of the real and imaginary parts of the pseudodielectric function (top) and the dielectric function (bottom) of bulk Ge from 10 K to 738 K. The arrows indicate changes from the measurement at 10 K (dashed) to 738 K.

Figure S2 shows the thickness of the native oxide layer on top of the Ge substrate at temperatures between 10 K and 738 K, obtained as explained in Ref. 6. The measurements were taken in approximately 25 K steps starting at 82 K and going up to 738 K. Formation of ice caused the increase of the oxide layer thickness between 82 K and room temperature. The decrease at temperatures above 300 K is due to degassing while at the highest temperatures oxidation or an increase in surface roughness leads to a growth in thickness. At temperatures above 650 K the band gap shift towards a region of increased noise and therefore the results for the thickness are less accurate. After the measurement at 738 K the heater was turned off to let the sample cool down to room temperature and further down to 10 K using liquid He. The larger oxide thickness at this temperature can be explained by condensation of nitrogen and oxygen.

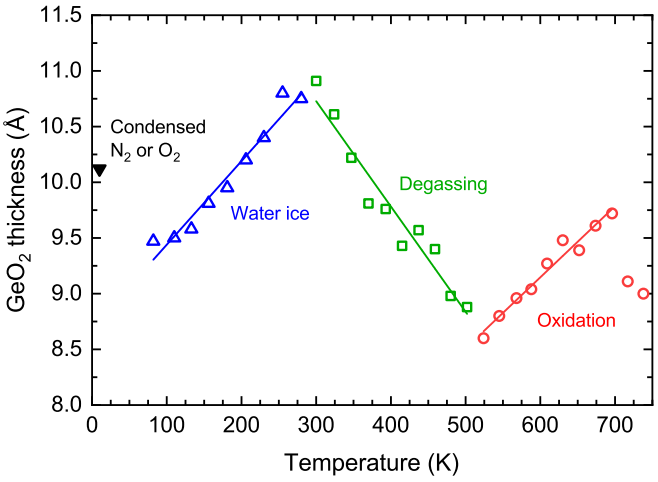

FIG. S2. Thickness of the native oxide layer with respect to temperature determined from the data sets plotted in Fig. S1. The changes of the oxide thickness are explained in the text.

At 10 K, several measurements between 0.5 eV and 1.7 eV were taken using step sizes between 0.5 meV and 10 meV and slit widths of 0.5 mm, 1 mm and 2 mm. The corresponding oxide thicknesses are shown in Fig. S3 as a function of time, where the time equal zero is defined to be the completion of the first measurement (10 meV, 2 mm). The increase of the GeO_2-thickness with time can be explained by a gain of O_2 or N_2 condensate.

In the region below 1 eV the level of noise increases as the temperature goes up due to black body radiation. This disturbs our data in the region of the band gap at temperatures above 500 K. To suppress this effect, an

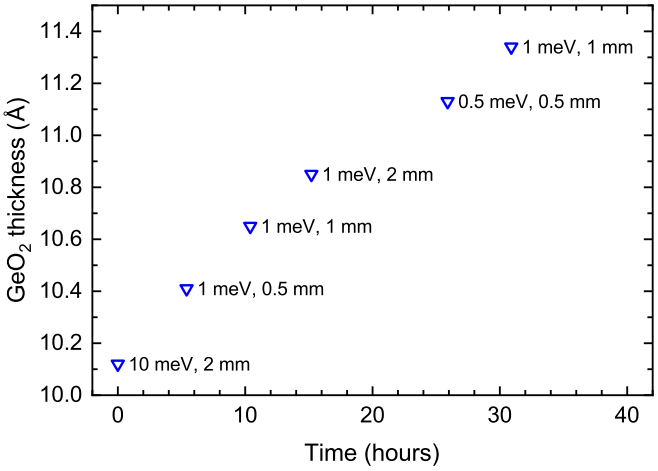

FIG. S3. Thickness of the native oxide layer of measurements with various step size (0.5 meV to 10 meV) and slit width (0.5 mm to 2 mm) at 10 K as function of time.

iris was placed behind the exit window of the cryostat for the data sets plotted in Fig. 2. This significantly improved the quality of the data in the region of the band gap, as demonstrated in Fig. S4 showing the ellipsometric angles at 583 K with and without the iris.

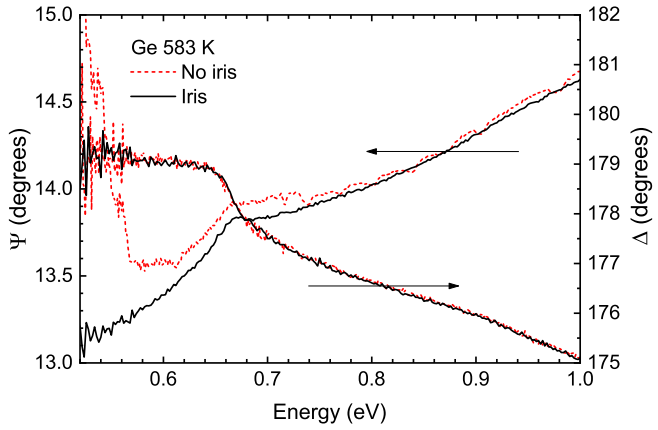

FIG. S4. Ellipsometric angles Ψ and Δ of Ge at 583 K using an iris attached to the outside of the exit window of the cryostat (solid) compared to not using an iris (dashed).

S2. ANALYSIS IN RECIPROCAL SPACE

From the RS analysis one can determine the CP parameters[25] as was done in Ref. 47 for 0D and 1D line shapes. In the case of a 3D line shape some issues arise which require further considerations. The amplitudes C_n of the Fourier coefficients for a CP line shape (Eq. (1)) can be expressed as[27]

$$\ln C_n = \ln \frac{A}{\Delta E^{\mu+\kappa}\Gamma(\mu)} - \frac{n\Gamma}{\Delta E} + (\mu+\kappa-1)\ln n, \quad \text{(S1)}$$

where $\Gamma(\mu)$ is the gamma function and κ is the order of differentiation. The parameters A, Γ and μ are defined in Eq. (1) and n and ΔE are explained in Sec. III B. A linear dependence of C_n on n is given for $\kappa = 0$ and $\mu = 1$, i.e. a 0D line shape, as well as for the first derivative of a 2D line shape ($\mu = 0$).[47] Expression (S1), which was derived using fractional differentiation with respect to E by order $\mu - 1$,[27] is problematic for $\mu < 0$ because $\Gamma(-1/2) < 0$. One might consider deriving a corresponding expression for $\mu < 0$ using fractional integration, for example utilizing Cauchy's formula for repeated integrals for real $p > 0$[48]

$$\frac{d^{-p}}{dt^{-p}} f(t) = \frac{1}{\Gamma(p)} \int (t-\tau)^{p-1} f(\tau) d\tau. \quad \text{(S2)}$$

S3. CRITICAL POINTS E_0 AND $E_0 + \Delta_0$

Figure S5 shows the real and imaginary part of the pseudo-DF around E_0 and $E_0 + \Delta_0$ at 10 K measured using a step size of 1 meV and a slit width of 1 mm. The DF corrected for the oxide thickness of 11.3 Å shown in Fig. S3 and fitted using the parametric semiconductor model is plotted in Fig. 3 together with an independent fit at each energy (dashed line). The vertical lines in both graphs mark the energies of E_0 and $E_0 + \Delta_0$ determined from the parametric semiconductor model fit.

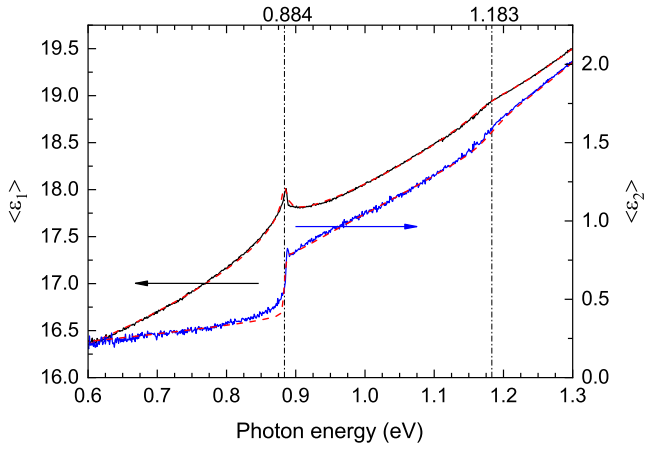

FIG. S5. Real and imaginary parts of the pseudodielectric function of bulk Ge at 10 K. The dashed lines show the fit to the data using a parametric semiconductor model.

The variation of the band gap energy with temperature was fitted by Varshni[9] via the relation

$$E(T) = E_{g,0} - \frac{\alpha T^2}{T+\beta}, \quad \text{(S3)}$$

where $E_{g,0}$ is the energy of the band gap at 0 K and α and β are constants. The result from fitting Eq. (S3) to the energies obtained by the PS, RS and SD methods are plotted in Fig. S6 with the fitting parameters listed in Tab. SI. Varshni's equation is an approximation of Eq. (8) which can be derived by substituting the power series of $e^{\theta_K/T}$ to second order in T into the Bose-Einstein factor. This yields the relations

$$E_{g,0} = E_a - E_b, \tag{S4}$$

$$\alpha = \frac{2E_b}{\theta_B}, \tag{S5}$$

$$\beta = \theta_B. \tag{S6}$$

To compare both relations, the energies $E_{g,0}$ are calculated from the Bose-Einstein fitting parameters given in Tab. I and are found to be between 0.88 eV and 0.89 eV for the energies determined by the PS, RS and SD methods as well as for McLean's data. The parameters α are in the order of 5×10^{-4} eV/K (PS, RS, SD) and 4×10^{-4} eV/K (McLean). The largest deviation is found for the effective phonon energy, i.e. β is about one third smaller than θ_B.

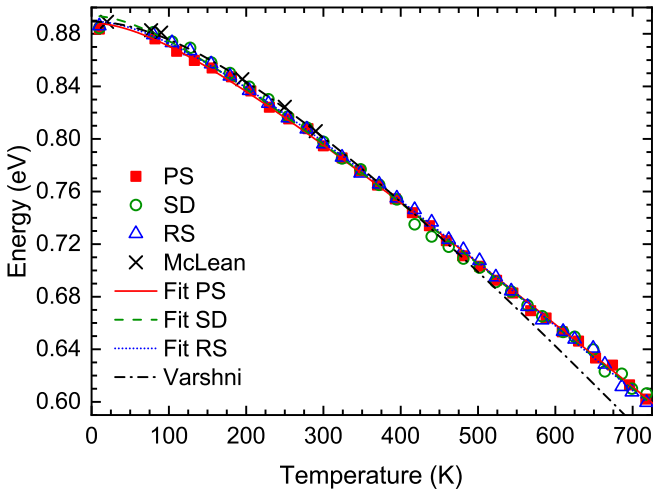

FIG. S6. Temperature dependence of the E_0 energies determined by a parametric semiconductor model (PS), a second derivative (SD) and a reciprocal space (RS) analysis. The crosses show the data from Ref. 8 (McLean). The lines represent the best fits to the data using Eq. (S3) and the results from Ref. 9 (Varshni, dash-dotted). The fitting parameters are listed in Tab. SI.

S4. CRITICAL POINTS E_1 AND $E_1 + \Delta_1$

The CPs E_1 and $E_1 + \Delta_1$ correspond to interband transitions along the (111) direction of the Brillouin zone. The temperature dependence of their energies determined from the second derivatives of the dielectric function assuming a 2D line shape[5]

$$\epsilon(\omega) = B - Ae^{i\phi} \ln(\hbar\omega - E + i\Gamma) \tag{S7}$$

are plotted in Fig. S7 together with the energies obtained from the PS model. The corresponding second derivatives of the real and imaginary parts of the DF at 10 K are shown in Fig. S8. The fits to the E_1 and $E_1 + \Delta_1$ energies of the present work using derivatives agree with the ones from Ref. 6 while the results from the PS model deviate significantly for both CPs.

TABLE SI. Parameters E_{g0}, α and β obtained from fitting Eq. (S3) to the temperature dependent energies of E_0 determined by the parametric semiconductor model (PS), the analysis in reciprocal space (RS) and the second derivative (SD) method compared with the results from Ref. 9.

	$E_{g,0}$ (eV)	α (10^{-4} eV/K)	β (K)
PS[a]	0.888 ± 0.002	5.0 ± 0.1	184 ± 18
RS[a]	0.890 ± 0.002	5.2 ± 0.1	213 ± 18
SD[a]	0.894 ± 0.003	5.0 ± 0.1	159 ± 26
Ref. 9	0.8893	6.842	398

[a]Present work.

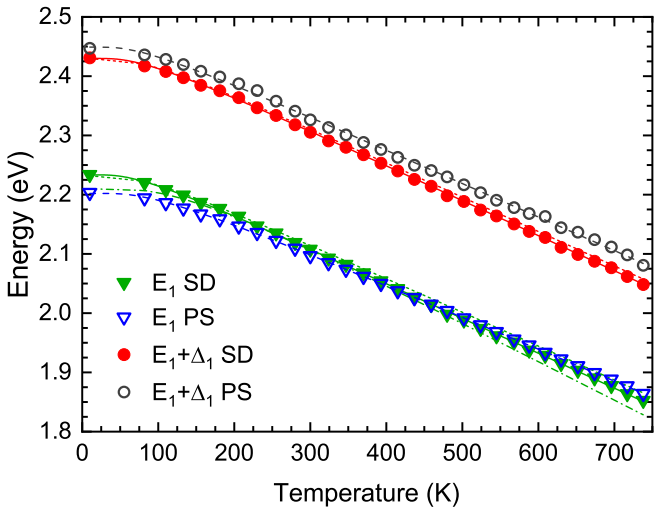

FIG. S7. Temperature dependence of the E_1 (triangles) and $E_1 + \Delta_1$ (circles) energies determined by an analysis of the second derivatives of the dielectric function (solid) and by a parametric semiconductor model (open). The lines show the fit to the data using Eq. (8) with parameters in Tab. I. The dotted lines show the results from Ref. 6 and the dash-dotted one shows the fit to E_1 from Ref. 5.

Figure S9 shows the spin orbit splitting Δ_1 obtained from the SD analysis with an average and standard deviation of $\Delta_1 = (199 \pm 2)$ meV which compares well with the value in Ref. 6.

TABLE SII. Broadening parameters Γ_1, Γ_2, θ_B and the effective phonon energy E_{ph} obtained from fitting Eq. (9) to the broadening as function of temperature of the E_1, $E_1+\Delta_1$, E_0' and E_2 CPs determined from an analysis of the second derivatives of the dielectric function. The parameters marked (f) of this work and of Ref. 6 were fixed during the fit.

	Γ_1 (meV)	Γ_2 (meV)	θ_B (K)	$E_{ph} = k_B \cdot \theta_B$ (meV)
E_1 [a]	6 ± 2	25 ± 3	341 ± 34	29 ± 3
E_1 (Ref. 6)	11 ± 1	14.2 ± 0.3	218 ± 14	19 ± 1
E_1 (Ref. 5)	12 ± 9	25 ± 3	376	32
$E_1+\Delta_1$ [a]	14 ± 1	20(f)	250(f)	22(f)
$E_1+\Delta_1$ (Ref. 6)	22 ± 3	15.1 ± 0.6	218(f)	19(f)
$E_1+\Delta_1$ (Ref. 5)	9 ± 8	43 ± 5	484	42
E_0' [a]	3.34 ± 0.02	0.15 ± 0.02	581 ± 42	50 ± 4
E_2 [a]	19 ± 14	53 ± 17	443 ± 41	38 ± 4
E_2 (Ref. 6)	38 ± 2	22.1 ± 0.5	217(f)	19(f)
E_2 (Ref. 5)	8 ± 5	69 ± 3	499	43

[a] Present work.

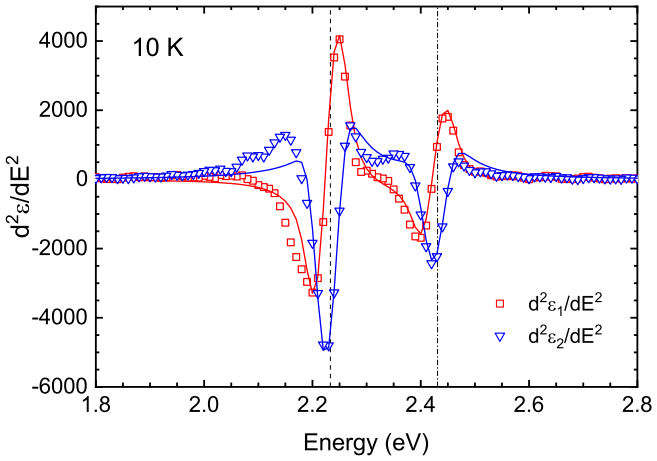

FIG. S8. Second derivatives of the real (squares) and imaginary (triangles) part of Ge at 10 K showing E_1 (2.22 eV) and $E_1+\Delta_1$ (2.4 eV). The solid lines show the best fit to the data assuming a two-dimensional line shape and the vertical lines indicate the E_1 and $E_1+\Delta_1$ energies.

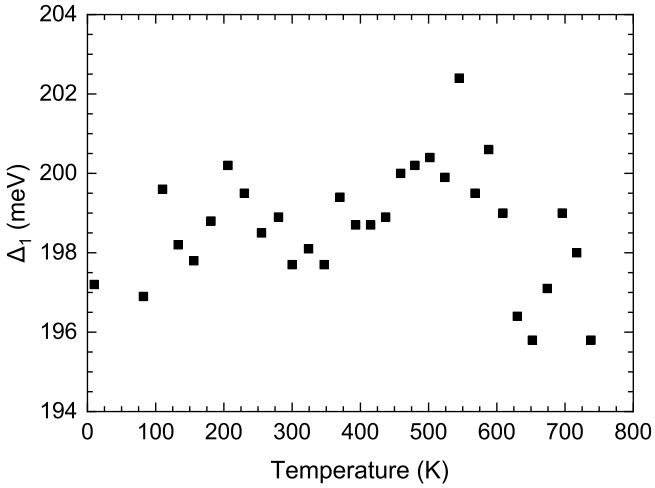

FIG. S9. Spin orbit splitting Δ_1 versus temperature obtained from the second derivative analysis.

The broadening of the E_1 and $E_1+\Delta_1$ CPs is shown in Fig. S10 with respect to temperature. The solid lines show the fits to the data with the parameters plotted in Tab. SII in comparison to the fits from Refs. 5 and 6.

During the fit of $\mathrm{d}^2\epsilon_1/\mathrm{d}E^2$ and $\mathrm{d}^2\epsilon_2/\mathrm{d}E^2$ the excitonic phase angles of E_1 and $E_1+\Delta_1$ were forced to have the same values. Their temperature dependence is shown in Fig. S11 and agree with the results of Ref. 6. The amplitudes of E_1 and $E_1+\Delta_1$ are plotted in Fig. S12.

S5. CRITICAL POINTS AT HIGHER ENERGIES

The parameters of CPs at energies above 3 eV ($\bar{E}_0'$ and E_2) were determined by the SD method and compared to the results from Refs. 5 and 6 (see Tabs. I and SII). Furthermore, as already shown in Refs. 5 and 6, the amplitudes are found to be independent and the phase angle decreases with temperature.

S6. DISCUSSION

The agreement with previous work[5,6] of the CP parameters of E_1 and $E_1+\Delta_1$, as well as CPs at higher energies ($\bar{E}_0'$ and E_2, see Tabs. I and SII), motivated us to apply the SD analysis also to the direct band gap. However, the results acquired for the broadening of E_0 (Fig. 8) show a larger variation and the E_0 phase angles do not show a clear temperature dependence. We suspect the reason for the lower precision and accuracy in the case of the direct band gap lies in its excitonic character. Therefore, a more detailed study of the band gap taking into account excitonic effects is required.

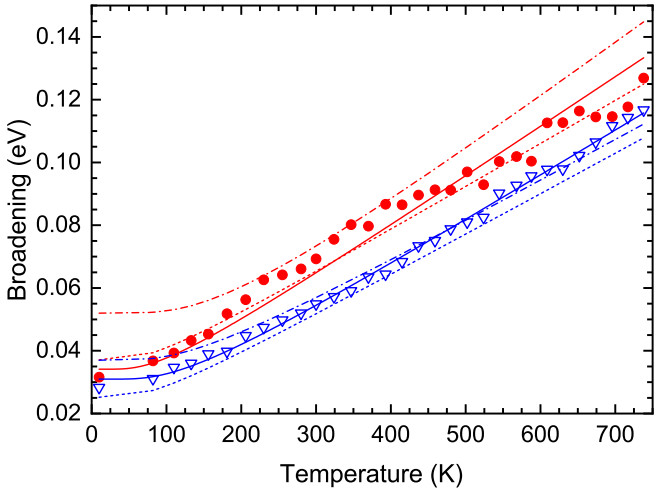

FIG. S10. Temperature dependence of the broadening of E_1 ($\bigtriangledown$) and $E_1+\Delta_1$ ($\bullet$) determined by an analysis of the second derivatives of the dielectric function. The solid lines show the fit to the data using Eq. (9) with parameteres in Tab. SII. The dotted lines show the results from Ref. 6 and the dash-dotted from Ref. 5.

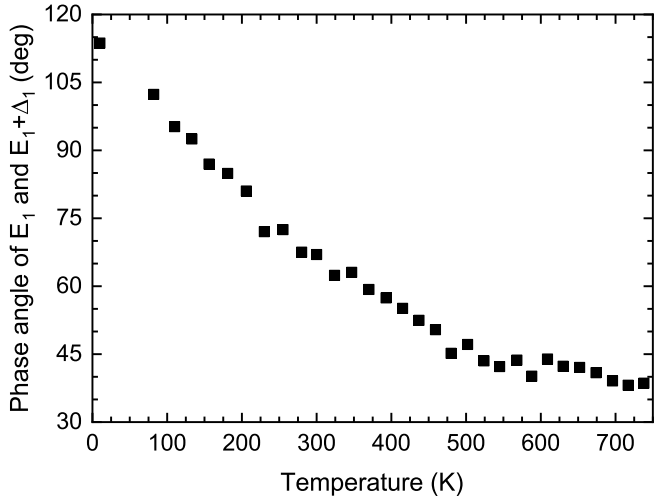

FIG. S11. Temperature dependence of the excitonic phase angle of E_1 and $E_1+\Delta_1$ determined from the second derivatives of the dielectric function.

Recent work by Menéndez et. al.[49] presents a thorough study of the indirect band edge of bulk Ge considering the resonant character of the indirect gap, which is only 0.1 eV below the direct gap, together with including excitonic effects.

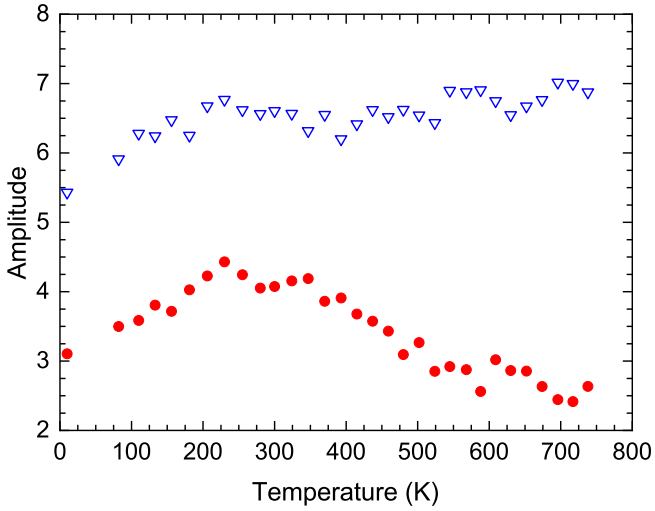

FIG. S12. Amplitudes of E_1 ($\bigtriangledown$) and $E_1+\Delta_1$ ($\bullet$) determined by a second derivative analysis.

ADDITIONAL REFERENCES

[47] L. F. Lastras-Martínez, R. E. Balderas-Navarro, J. Ortega-Gallegos, A. Lastras-Martínez, J. M. Flores-Camacho, and K. Hingerl, J. Opt. Soc. Am. B **26**, 725 (2009).

[48] I. Podlubny, *Fractional Differential Equations: An Introduction to Fractional Derivatives, Fractional Differential Equations, to Methods of Their Solution and some of Their Applications*, p. 64 (Academic, San Diego, 1999).

[49] J. Menéndez, D. J. Lockwood, J. C. Zwinkels, and M. Noël, Phys. Rev. B **98**, 165207 (2018).